Interconnected Nanoporous Polysulfone by Self-Assembly of Randomly-Linked Copolymer Networks and Linear Multi-Blocks

Jaechul Ju, Ryan C. Hayward*

Chemical and Biological Engineering, University of Colorado Boulder, Boulder, CO 80303

ABSTRACT:

Porous materials have attracted considerable attention due to their versatile applications, especially in water purification. Materials with interconnected nanoporous structures are distinguished by their high degree of porosity and resistance to clogging, as well as their insensitivity to nanostructural orientation. Previously work on randomly-linked blocky copolymer systems has shown that they can effectively produce disordered cocontinuous nanostructures, which upon removal of one component yield interconnected nanoporous materials with well-controlled pore sizes. However, the cocontinuous nanomaterials previously developed using polystyrene (PS) and poly(D,L-lactic acid) (PLA) strands, and the resulting interconnected nanoporous PS monoliths, were found to be far too brittle to enable practical use as membranes. Here, we study the self-assembly of randomly-linked copolymer networks prepared using blocks of the engineering polymer polysulfone (PSU), instead of PS. A wide cocontinuous regime (spanning 40 wt. %) was found for randomly end-linked copolymer networks (RECNs) constructed from PSU and PLA strands, via a combination of mechanical testing, gravimetric analyses, small-angle X-ray scattering, and scanning electron microscopy. The PSU/PLA cocontinuous nanomaterial with symmetric composition showed 2.4 times higher Young's modulus and ~ 100 times greater toughness than a corresponding PS/PLA sample. The interconnected nanoporous PSU fabricated after etching of PLA even exhibited a 1.6 times greater toughness than PS/PLA prior to PLA removal. To facilitate the production of thin films of cocontinuous nanomaterials, we applied solution-processable randomly-linked linear multi PSU/PLA blocks (RLMBs) onto ultrafiltration membranes via spin coating. The interconnected nanoporous PSU thin film generated by selectively etching PLA was found to effectively reject 50 nm diameter particles without significantly compromising permeability. This discovery presents a valuable addition to the existing techniques used to fabricate PSU

membranes. In contrast to traditional methods, which are sensitive to processing conditions, produce a wide range of pore sizes, and offer limited adjustability of pore size, the current technique is anticipated to enable interconnected PSU membranes with more uniform and tailorable porosity.

KEYWORDS: *disordered cocontinuous nanomaterials, randomly end-linked copolymer networks, randomly-linked linear multiblock copolymers, engineering polymer, polysulfone*, *solution/melt processing, ultrafiltration membrane*

1. INTRODUCTION

The pressing challenges associated with global water scarcity motivate the development of high-performance filtration membranes.[1–3] Ultrafiltration membranes, with pore sizes ranging from 1 to 100 nm, are especially important for drinking water and wastewater treatment.[3,4] These sizes correspond to the hydrodynamic sizes of various contaminants, including viruses, microbes, and colloidal particles.[5,6] Through the process of polymer microphase separation, it is possible to achieve these precise pore sizes, leading to significant advancements in ultrafiltration membrane technology.[7]

Ultrafiltration membranes are typically produced via non-solvent induced microphase separation (NIPS), yielding interconnected porous structures with a gradient in pore sizes that optimize selectivity and permeability.[8,9] However, a significant challenge of NIPS is the precise control of pore size and distribution, as it is highly sensitive to fabrication conditions.[5] To address this, the self-assembly of block copolymers with NIPS (SNIPS) was introduced, combining methods to form selective layers with uniform pores ranging from 10 to 100 nm.[10–12] Despite its advantages, SNIPS remains sensitive to the kinetics of fabrication processes, such as the solvent evaporation rate.[5] For instance, selective layers with cylindrical pores are highly affected by the evaporation rate, leading to variations in the alignment and orientation of porous domains.[13,14] This variability can impair membrane performance, including permeability.

In response to these fabrication challenges, interconnected nanopores have come to the forefront, prized for their uniformity and efficiency across all angular orientations due to 3D percolation. This characteristic significantly mitigates the impact of varied processing conditions. Additionally, these structures maintain comparable selectivity to other isoporous nanostructures,[15–17] enhance permeability over hexagonal structures due to enlarged pore volumes,[18,19] and improve clogging resistance by reducing pore dead ends through pore

connectivity.[20]

Diverse methods have been developed to create cocontinuous phases, including thermodynamically based techniques that are not sensitive to processing conditions. Typically, AB diblocks[21] and other block copolymers[22,23] form cocontinuous phases. However, the cocontinuous window is limited to narrow composition ranges (i.e., $\lesssim$ 5 vol. %), although the stability of these structures can be enhanced by molecular weight dispersity.[24,25] Additionally, kinetic trapping strategies further support the formation of these structures by quenching transient cocontinuous morphologies.[26] These strategies, however, require precise control over temperature,[27–29] solvent evaporation rates,[30,31] humidity,[32] and crystallization.[33] A notable method, polymerization-induced microphase separation (PIMS), also supports the development of these structures, albeit with some sensitivity to balancing separation and polymerization kinetics.[34]

Recent developments in methods have made the fabrication of interconnected nanoporous layers accessible. Techniques like crosslinking above the order-to-disorder transition temperature of (T_{ODT})[15–17] and quenching to vitrify disordered structures[35,36] have been designed to ease fabrication, even with the challenges of achieving the necessary polymer composition symmetry for cocontinuity. Our group has explored microphase separation of randomly end-linked copolymer networks (RECNs), where cocontinuous nanomaterials and/or interconnected nanoporous polymers have been formed over composition ranges as wide as 30 – 45 wt. %.[37–39] This approach shows relatively little sensitivity to kinetics, since the disordered morphology with well-defined domain spacing *d* appears to represent an equilibrium morphology (or as close as is possible given the presence of crosslinking. In addition, we have studied randomly-linked linear multiblock copolymers (RLMBs),[40] achieving cocontinuous nanostructures over a somewhat narrower composition range of $\approx$ 20 wt. %, but with the

offsetting benefit of enabling solution processing. Despite the straightforward access to interconnected nanoporous structures provided by this approach, we have so far relied on brittle polystyrene (PS) strands to form the pore walls, thus limiting practical applications.

To enhance the potential applicability of interconnected nanoporous membranes generated from randomly-linked copolymer architectures, we here focus on replacing PS with the engineering polymer polysulfone (PSU), known for its superior mechanical, thermal, and chemical stability.[41] We combined PSU and PLA strands via random linking to yield network (RECN) and linear (RLMB) architectures.[37,40] Through mechanical, gravimetric, small-angle X-ray scattering (SAXS), and scanning electron microscopy (SEM) analyses, we identified a broad cocontinuous range in PSU/PLA RECNs (≈ 40 wt. %). These PSU/PLA nanostructures exhibited enhanced Young's modulus and toughness, surpassing those of PS/PLA materials. We then prepared interconnected nanoporous PSU thin films via solution-processable RLMBs architectures, followed by selective etching of PLA to yield ultrafiltration membranes that exhibited high size selectivity without significantly reducing permeability of the macroporous supports.

2. EXPERIMENTAL SECTION

2.1. Polymer Synthesis

2.1.1. Materials. Bisphenol A (BPA, ≥ 99 %), 4,4-dichlorodiphenyl sulfone (DCDPS, 98 %), potassium carbonate (K_2CO_3, ≥ 99.0 %), pentaerythritol tetrakis(3-mercaptopropionate) (PETMP, > 95 %), acryloyl chloride (≥ 97 %), triethylamine (TEA, ≥ 99.5 %), anhydrous N-methyl-2-pyrrolidone (NMP, 99.5 %), anhydrous dichloromethane (DCM, ≥ 99.8 %), anhydrous ethylene glycol (99.8 %), and 1,8-diazabicyclo[5.4.0]undec-7-ene (DBU, 98 %)

were purchased from Sigma-Aldrich (St. Louis, MO, USA). D,L-lactide was obtained from Corbion (Lenexa, KS, USA), and ethylene glycol bis(3-mercaptopropionate) (> 98.0 %) was purchased from Tokyo Chemical Industry (TCI America, Portland, OR, USA). Toluene (≥ 99.5 %), sodium bicarbonate ($NaHCO_3$, ≥ 99.7 %), sodium chloride (≥ 99.0 %), hydrochloric acid (HCl, 36.5 %), methanol (MeOH, ≥ 99.9 %), and benzoic acid (≥ 99.5 %) were provided from Fisher scientific (Hampton, NH, USA). Di-acrylate terminated poly(D,L-lactic acid) (Ac-PLA-Ac) of 6.0 kg/mol by nuclear magnetic resonance (NMR) was obtained from Advanced Polymer Materials Inc. (Dorval, Montreal, Canada). Gold nanoparticles (30 and 50 nm) supplied in 0.1 mM phosphate buffered saline (≥ 95 %) were purchased from Alfa Aesar (Haverhill, MA, USA). d-Chloroform was purchased from Cambridge Isotope Laboratories (Tewksbury, MA, USA). All materials were used as received without additional purification.

2.1.2. Di-hydroxy Terminated Polysulfone (HO-PSU-OH). To synthesize HO-PSU-OH via polycondensation, a modest excess of BPA over DCDPS was used, with r = [chloride] / [alcohol] = 0.944, to ensure hydroxy end-groups. To achieve a desired molecular weight (≈ 10 kg/mol), the target degree of polymerization, as described by the Carothers equation $N_{PSU} = \frac{1+r}{1+r-2rp}$,[42] would require a conversion of $p \approx 0.98$, where N_{PSU} denotes the number-average degree of polymerization of PSU. BPA (2.85 g, 12.5 mmol), DCDPS (3.46 g, 11.8 mmol), and K_2CO_3 (2.07 g, 15 mmol) were added with a magnetic stirrer into a Schlenk flask connected with a nitrogen inlet, Dean-Stark trap, and reflux condenser. Under nitrogen purge, anhydrous NMP (26 mL) and toluene (13 mL) were added to the reactor. The temperature increased to 155 ℃ and sat for 4 h. Then the temperature was increased to 175 ℃ and maintained for 16 h. Once the reaction was finished, the temperature was cooled down to room temperature, and then a slight amount of DCM was added to dissolve the precipitated PSU since the solution had

become concentrated during polycondensation. The concentrated polymer solution was transferred dropwise to cold MeOH for re-precipitation. This step was repeated by re-dissolving the PSU powder with DCM and re-precipitating it in cold MeOH. The produced white powder was dried in vacuo at 100 °C overnight. The molecular weight and dispersity were characterized by NMR (Figure S1) as M_n = 8 kg/mol, corresponding to $p \approx 0.97$ from the Carothers equation, and by size-exclusion chromatography (SEC), which showed a dispersity ($Đ$) of 1.8 (see Supporting Information, Section 2 for full details).

2.1.3. Di-acrylate Terminated Polysulfone (Ac-PSU-Ac). To obtain Ac-PSU-Ac, acrylate end-functionalization was achieved by our previous method.[38] The dried HO-PSU-OH (2 g, 0.24 mmol) was dissolved in 30 mL of anhydrous DCM in a dried round-flask with a magnetic stir bar, then kept the flask in an ice bath with nitrogen gas purging for at least 20 m. Under a nitrogen gas environment, acryloyl chloride (400 μL, 4.88 mmol) and TEA (680 μL, 4.88 mmol) were each added dropwise to the stirring polymer solution, respectively. The reaction continued overnight. Once the reaction was complete, the solution was washed with 1 M HCl in H_2O, concentrated $NaHCO_3$, and concentrated brine in turn. The product was re-precipitated into cold MeOH. The functionality of the acrylate group was calculated to be 1.92 by NMR (Figure S2).

2.1.4. Di-hydroxy Terminated Poly(D,L-lactic acid) (HO-PLA-OH). To synthesize HO-PLA-OH, ring-opening polymerization of D,L-lactide was performed with dried chemicals and glassware in an argon-filled glove box. In a glove box filled with argon gas, D,L-lactide (3.3 g, 22.5 mmol) and ethylene glycol (38 μL, 0.3 mmol) were dissolved in anhydrous DCM (22.5

mL) inside a dried round-flask equipped with a magnetic bar. Gentle heat using a heat gun was applied to make a homogenous solution. Then, DBU catalyst (116 μL, 0.75 mmol) was inserted at once during vigorous stirring. The reactor was meticulously sealed to maintain its dryness and then taken out of the glove box. The reaction continued with stirring at room temperature for 3 h. Once the reaction was complete, the catalyst was quenched with excess benzoic acid (229 mg, 1.87 mmol). The product solution was concentrated by air-blowing and then re-precipitated with cold MeOH. This step was repeated by re-dissolving the PLA powder with DCM and re-precipitating it with cold MeOH. The purified PLA was dried in vacuo at 40 °C overnight. The molecular weight was characterized by NMR as M_n = 11 kg/mol (Figure S3), and the dispersity was measured by SEC as $Đ$ = 1.2, respectively (Supporting Information, Section 2 for full details).

2.1.5. Di-acrylate Terminated Poly(D,L-lactic acid) (Ac-PLA-Ac). To obtain Ac-PLA-Ac, the same acrylation procedure was followed, as shown for PSU, and its end-group functionality was measured to be 1.86 by NMR (Figure S4).

2.2. Random Copolymer Systems of PSU/PLA

2.2.1. PSU/PLA RECN Preparation. The RECN samples are named $SU_{MPSU}L_{MPLA}$-ω_{PLA}, where the subscripts indicate the molecular weights (g/mol) of each strand and ω_{PLA} refers to the weight percent of PLA. $SU_{8k}L_{11k}$ RECNs were synthesized by thiol-Micheal couplings. Firstly, the stock solutions of Ac-PSU-Ac, Ac-PLA-Ac, PETMP, and TEA were fabricated with NMP at 200, 200, 50, and 50 mg/mL, respectively. To prepare the final solution, the stock solutions of PSU and PLA were mixed in ratios corresponding to the desired weight ratios,

with a molar ratio of [acrylate] : [thiol] = 1 : 1. The solution concentration was set at 150 mg/mL, accordingly with the addition of NMP. Once it was homogenously mixed, TEA (1 equiv. of thiol) was added to the solution, immediately followed by vigorous vortexing. The reaction continued for 1 d. Once the reaction was complete, the fabricated samples were then allowed to adopt their preferred microphase separated nanostructures through slow evaporation of solvent at room temperature in atmospheric condition overnight, followed by drying in vacuo at 100 ℃ for 1 d, and then thermally annealing at 190 ℃ for 1 d under a closed chamber filled with argon gas (Scheme 1).

Scheme 1. Polymers and crosslinkers applied for RECNs and the processing route for an interconnected nanoporous PSU monolith.

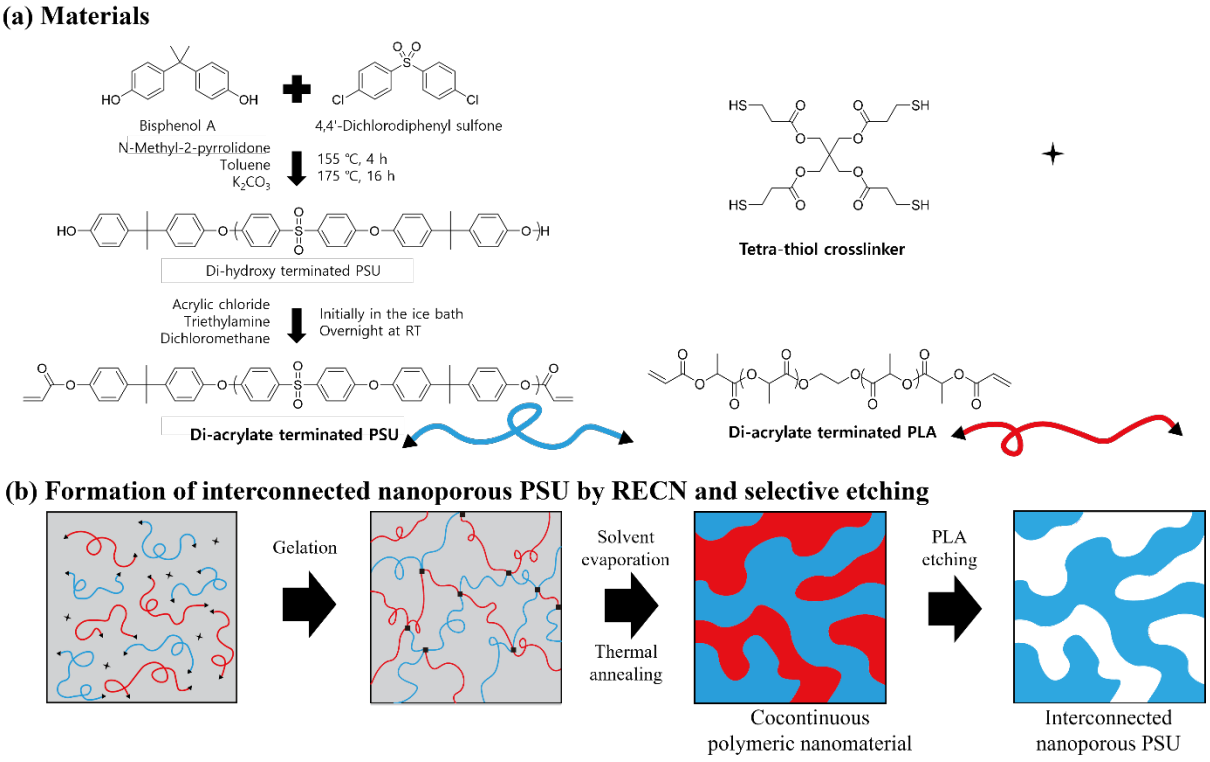

2.2.2. PSU/PLA RLMB Preparation. The PSU/PLA RLMB with the symmetric composition ($SU_{8k}L_{6k}$(M)-50) was synthesized by randomly linking Ac-PSU-Ac of 8 kg/mol and Ac-PLA-Ac of 6 kg/mol with ethylene glycol bis(3-mercaptopropionate) via thiol-Michael coupling. The molecular weight of PLA was selected as 6 kg/mol to target pore sizes smaller than 50 nm for filtration tests involving 30 nm and 50 nm Au nanoparticles. Firstly, the stock solutions of Ac-PSU-Ac, Ac-PLA-Ac, di-thiol chain extender, and TEA were fabricated with NMP at 200, 200, 50, and 50 mg/mL, respectively. To prepare the final solution, the stock solutions of PSU and PLA were mixed at $\omega_{PLA} = 0.5$, with a molar ratio of [acrylate] : [thiol] = 1 : 1. The solution concentration was set at 150 mg/mL, accordingly with the addition of NMP. Once it was homogenously mixed, TEA (1 equiv. of thiol) was added to the solution, immediately followed by vigorous vortexing. The reaction continued for 3 d at 60 °C. Once the reaction was complete, the resulting product was transferred dropwise to cold MeOH for re-precipitation. The produced white powder was dried in vacuo at 40 °C overnight.

2.3. Ultrafiltration Membrane Preparation. The polymer $SU_{8k}L_{6k}$(M)-50 was dissolved in chlorobenzene at a concentration of 2 wt.%. The choice of solvent was made based on the following requirements: good solvent for the polymer, and a bad interaction with both supporting membranes and a filling solvent. To begin the fabrication process, a porous polyethersulfone (PES) substrate was filled with water before the stock solution was dropped. Removing excess water from the PES substrate is an important step in controlling the thickness and uniformity of the spin-coated materials. The stock solution was then spin-coated onto the shiny side of the porous PES substrate, as this supporting membrane has a gradual variation in pore sizes. The shiny side has pores of ≈ 100 nm, while the matte side has pores of ~ 1 μm. The choice of the spin-coating side is crucial for creating bi-layer membranes with gradient pores,

where the pore sizes become larger from top to bottom (from the spin-coated to the other). This process ensured that the spin-coated solution would not infiltrate the supporting membrane with larger pores, which would lower its porosity and result in irregular and heterogeneous patterns of pore sizes instead of the desired gradient pattern. After spin-coating, the membranes were dried under ambient conditions for 10 m and then at 100 °C for 1 h. Subsequently, thermal annealing was performed at 190 °C for 3 h. It is worth noting that during the drying and annealing processes, it is common for spin-coated membranes to become curved or warped. This curvature typically occurs due to differences in drying rates and/or modulus mismatch of the materials used. To address this issue, substrates with a larger size, a diameter of 4.7 cm in our case, were used for the spin-coating process. Afterward, the membranes were punched into smaller discs with a diameter of 1.27 cm. This approach handles/minimizes the creation of curvatures curving membranes. These smaller discs were then inserted into the membrane testing cell for further analysis and evaluation (Scheme 2).

Scheme 2. Synthesis of PSU/PLA RLMBs and fabrication of the ultrafiltration membrane composed of the interconnected nanoporous PSU on the top of PES supporting substrate.

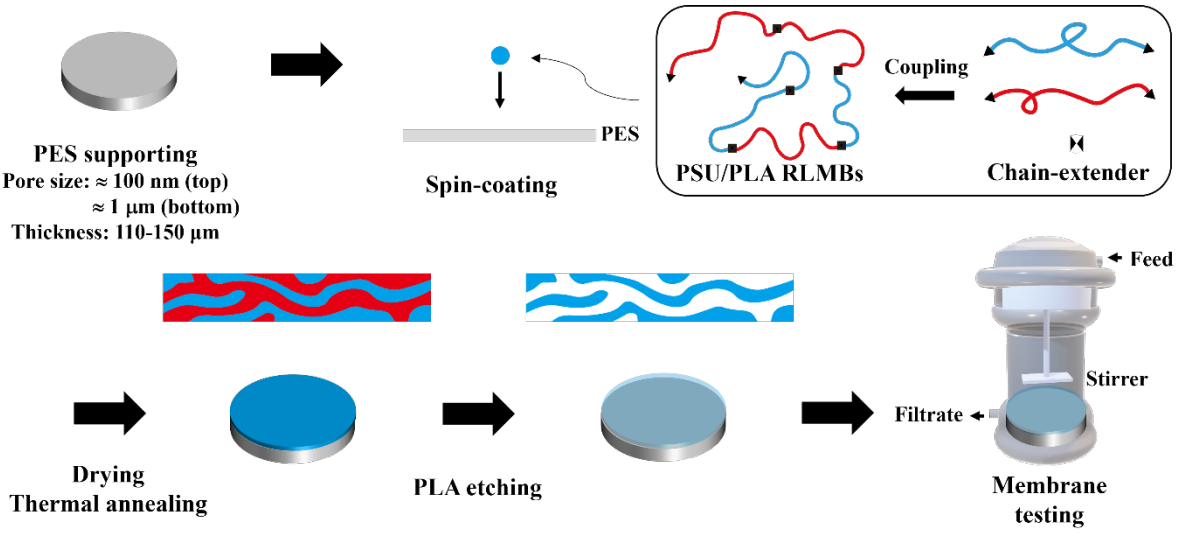

2.4. PLA Etching. The PSU/PLA RECNs and RLMBs were immersed in a 1 M NaOH in H_2O/MeOH at a 1 : 1 volume ratio for 1 d, followed by washing with a fresh mixture of H_2O and MeOH at a 1 : 1 volume ratio three times. The etched samples were dried under vacuum overnight.

3. RESULTS AND DISCUSSION

We began by examining self-assembly of RECNs constructed from PSU and PLA strands. To achieve microphase separation, a critical degree of segregation (χN), where χ is the Flory-Huggins interaction parameter between the polymers and $N = N_A + N_B$ is their combined degree of polymerization, of at least $\gtrsim$ 10 must be achieved, as found in a previous study of PS/PLA RECNs.[39] While we are not aware of any reports regarding the χ value between PSU and PLA, we chose a target strand molecular weight of ≈ 10 kg/mol, which is presumably long enough to induce microphase separation but short enough for them to homogeneously mix in a common solvent.

To identify the composition range over which cocontinuous nanostructures were formed, we determined the percolation thresholds for both PLA and PSU microphases. For PLA, we employed gravimetric analysis, leveraging the selective etchability of PLA. To determine the PSU percolation threshold, we compared Young's modulus values at 80 °C, which is below the glass transition temperature of PSU ($T_{g,\,PSU}$ = 176 °C as shown in Figure S8), but above that of PLA ($T_{g,\,PLA}$ ≈ 40 °C).[39] The gravimetric analysis was conducted by simply weighing $SU_{8k}L_{11k}$ before and after PLA etching. The y-axis in Figure 1a represents the decrease in mass Δm due to etching of PLA, normalized by the initial sample mass m_0, while the x-axis represents the PLA weight fraction in the RECN, such that the line $y = x$ corresponds

to full removal of PLA. For $SU_{8k}L_{11k}$-20, only a moderate amount of PLA was etched (19 %), indicating that most PLA domains were not percolated and thus remained unexposed to the etchant. In contrast, $SU_{8k}L_{11k}$-30 exhibited essentially complete etching of PLA, indicating full PLA percolation in this sample. Consequently, the threshold for robust PLA percolation is established at $\omega_{PLA} \approx 0.25$. Upon increasing the PLA content to $SU_{8k}L_{11k}$-70 or above, samples no longer remained mechanically intact and instead broke into many small pieces during PLA etching, suggesting a lack of PSU percolation at this composition.

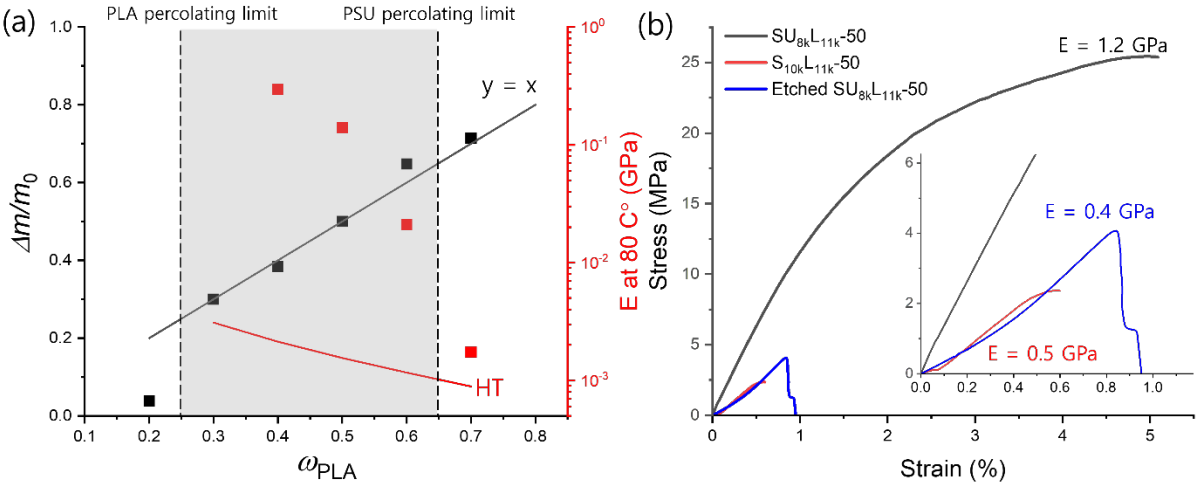

Figure 1. (a) The cocontinuous window (shaded gray region; ≈ 40 wt. % in width) for $SU_{8k}L_{11k}$ as defined by the boundaries for percolation of PLA and PSU (dotted lines) via gravimetric analysis and mechanical testing at 80 °C, respectively. (b) Comparison of the mechanical properties of $SU_{8k}L_{11k}$-50, $S_{10k}L_{11k}$-50 and etched $SU_{8k}L_{11k}$-50 at room temperature. $SU_{8k}L_{11k}$-50 shows 2.4 times higher Young's modulus and ~ 100 times greater toughness (8 times larger stretchability) than $S_{10k}L_{11k}$-50. The etched $SU_{8k}L_{11k}$-50 exhibits a 1.6 times greater toughness and stretchability than $S_{10k}L_{11k}$-50, while maintaining a similar Young's modulus.

Regarding the identity of the PSU percolation threshold, for large PSU contents (small ω_{PLA}), percolation of the glassy PSU phase leads to high (> 100 MPa) Young's modulus,[43] while in the case of pure PLA, we expect a rubbery modulus of ≈ 0.4 MPa, based on our previous measurement of pure PLA networks composed of the identical strands of PLA and crosslinker used in this study.[39] To capture the transition from dispersed to percolated PSU, we applied the Halpin-Tsai (HT) model, which is commonly used to predict the mechanical properties of composites of fillers (here, the dispersed PSU phase) in a matrix (continuous PLA phase).[44,45] For $\omega_{PLA} \lesssim 0.6$, the measured Young's modulus exceeds the predicted value by more than 10 times, strongly supporting that PSU is well-percolated for these samples. In contrast, the close proximity of the Young's modulus of $SU_{8k}L_{11k}$-70 to the HT prediction suggests that the PSU phase was dispersed or very weakly percolated. In concert with the observation of $SU_{8k}L_{11k}$-70 fragmentation upon etching of PLA, we therefore assign the threshold for robust PSU percolation at $\omega_{PLA} \approx 0.65$. Using the identified PLA and PSU boundaries, the cocontinuous window of $SU_{8k}L_{11k}$ was defined as being approximately 40 wt. % wide (i.e., from $\omega_{PLA} \approx 0.25 – 0.65$). We note that in previous work on PS/PLA RECNs, we have also employed nitrogen absorption porosimetry to help establish the percolation threshold of the PS phase.[37] However, due to the consistency found previously with the other methods employed here, and the relatively large amounts of sample required, we did not pursue these measurements here.

To test how the mechanical properties of the cocontinuous $SU_{8k}L_{11k}$ RECN compared to a cocontinuous PS/PLA RECN, we performed tensile tests on $SU_{8k}L_{11k}$-50 and $S_{10k}L_{11k}$-50 at room temperature (typically ≈ 20 °C). The strain-stress curves in Figure 1b show that the polysulfone-based $SU_{8k}L_{11k}$-50 had a Young's modulus of 1.2 GPa, toughness of 930 kN/m^2, and strain at break of 5.1 %. In contrast, $S_{10k}L_{11k}$-50 showed smaller values, i.e., Young's

modulus of 0.5 GPa, toughness of 8 kN/m^2, and strain at break of 0.6 %. The removal of the PLA phase to generate an interconnected nanoporous structure inevitably renders the material more brittle, since the pores act as stress concentrators, reducing the material's ability to bear loads.[46] Additionally, the introduction of pores reduces the effective elastic modulus since there is less material to resist deformation under load.[47] Notably, however, even after removal of PLA, the etched $SU_{8k}L_{11k}$-50 showed 1.6 times higher toughness and stretchability compared to the unetched $S_{10k}L_{11k}$-50 while having a similar Young's modulus. Conversely, the etched $S_{10k}L_{11k}$-50 sample exhibited extreme brittleness; it often broke even when handled gently with tweezers, precluding accurate measurements of mechanical properties. The improvement in mechanical properties suggests that interconnected nanoporous PSU, as well as PSU/PLA cocontinuous nanomaterials have greater potential for practical applications compared to their PS-based counterparts.

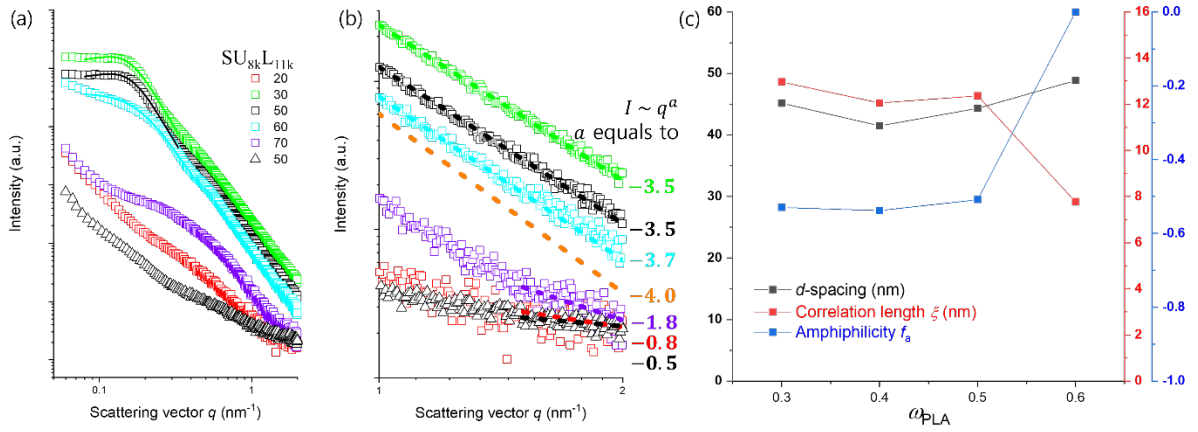

Figure 2. (a) SAXS patterns of $SU_{8k}L_{11k}$. Triangles: before PLA etching. Squares: after PLA etching. No characteristic or noticeable scattering patterns were observed in $SU_{8k}L_{11k}$ without PLA etching, possibly due to a very low difference in electron density between PSU and PLA. To maintain legibility, SAXS patterns for $SU_{8k}L_{11k}$-40 are omitted here but can be found in

Figure S9. (b) Exponent values obtained from power-law fitting in the Porod regime presented in Figure 2a, where values close to $a = -4$ (dashed orange line) suggest nanoporous structures with sharp interfaces for etched $SU_{8k}L_{11k}$-30, -50, and -60, while a value of – 1.8 for etched $SU_{8k}L_{11k}$-70 suggests a collapse and loss of porosity. (c) Values of *d*-spacing, ξ, and f_a obtained from TS fitting.

Additionally, we employed SAXS to gain further insight into the microphase separation and the cocontinuity range for $SU_{8k}L_{11k}$ (Figure 2a). Surprisingly, the $SU_{8k}L_{11k}$ RECNs prior to PLA etching showed no clear characteristic scattering features, as can be seen for $SU_{8k}L_{11k}$-50 (black triangles; see Figure S9 for the other compositions). We suspect that this must reflect a very small electron density contrast between PSU and PLA, rather than the absence of nanostructure. Indeed, after selective etching of PLA by immersion in a 1 M NaOH solution in H_2O/MeOH at a 1 : 1 volume ratio for 1 d, the scattering intensity dramatically increased, due to the much larger electron density contrast between PSU and vacuum. In addition, a characteristic shoulder emerged in the SAXS pattern (black squares), consistent with the presence of a disordered microphase separated structure. We note that here a relatively broad shoulder appears, whereas in our prior work on PS/PLA RECNs a more distinct, though still broad, peak was observed.[37–39] We suspect that one reason for the additional broadening of the patterns may be the use of PSU with high molecular weight dispersity due to its synthesis by step-growth polymerization. This behavior was found in samples containing 30 – 60 wt. % PLA, indicating the extraction of a considerable amount of PLA, while maintaining the original PSU nanostructure. In contrast, for $SU_{8k}L_{11k}$-20, only a weak increase in intensity was observed upon etching, suggesting that most PLA domains were embedded within a PSU matrix, leading to only a small amount of PLA extracted. Thus, the SAXS measurements of samples after PLA

etching indicate that the threshold for robust percolation of PLA lies between $SU_{8k}L_{11k}$ -20 and $SU_{8k}L_{11k}$ -30, consistent with the gravimetric results described above.

Furthermore, these broad characteristic patterns indicative of disordered morphologies were quantitatively analyzed using the Teubner-Strey (TS) model, which is commonly employed to describe the structure of bicontinuous microemulsions.[48] By fitting the data to the TS model, the following structural parameters were determined: (i) the *d*-spacing, representing the center-to-center distance between one polymer domain and a neighboring domain of the same material, (ii) the correlation length ξ, representing how rapidly electron density correlations decay spatially, and (iii) the amphiphilicity factor f_a, which indicates the stability of the microemulsion.[40,49] Values of *d*-spacing and ξ were found to be ≈ 50 and ≈ 10 nm, respectively, and were nearly independent of the copolymer composition (Figure 2c). In addition, the small value of the ratio $\xi / d \approx 0.20$ indicates a wide range of *d*-spacing dispersity, explaining why the characteristic shoulders were obtained instead of broad peaks.[50] The stability of cocontinuous phases can be evaluated through f_a value, and typically stable cocontinuous phases have a value of f_a between -1 and 0.[40,49,51] For $SU_{8k}L_{11k}$-30 to $SU_{8k}L_{11k}$-50, the f_a values are around -0.5, while for $SU_{8k}L_{11k}$-60, the value is close to zero but still slightly negative. For $SU_{8k}L_{11k}$-70, the significant reduction in *d*-spacing and the substantially broader and weaker scattering profile observed after PLA etching suggests a substantial collapse of the microphase separated morphology. While the SAXS data for etched $SU_{8k}L_{11k}$-30 to -60 agree well with the behavior $I \sim q^{-4}$ in the Porod regime (q $\gtrsim$ 0.7 - 2 nm^{-1} here) that is expected for nanoporous structures with sharp interfaces, the etched $SU_{8k}L_{11k}$-70 shows the scaling $I \sim q^{-1.8}$ (fitted over $q \approx 1.5$ - 2 nm^{-1} to avoid the tail of the characteristic scattering feature), indicating a substantial loss of porosity (Figure 2b).[52,53] This reflects a non-, or

weakly-percolated PSU, aligning with the previously established PLA threshold from measurements of Young's modulus.

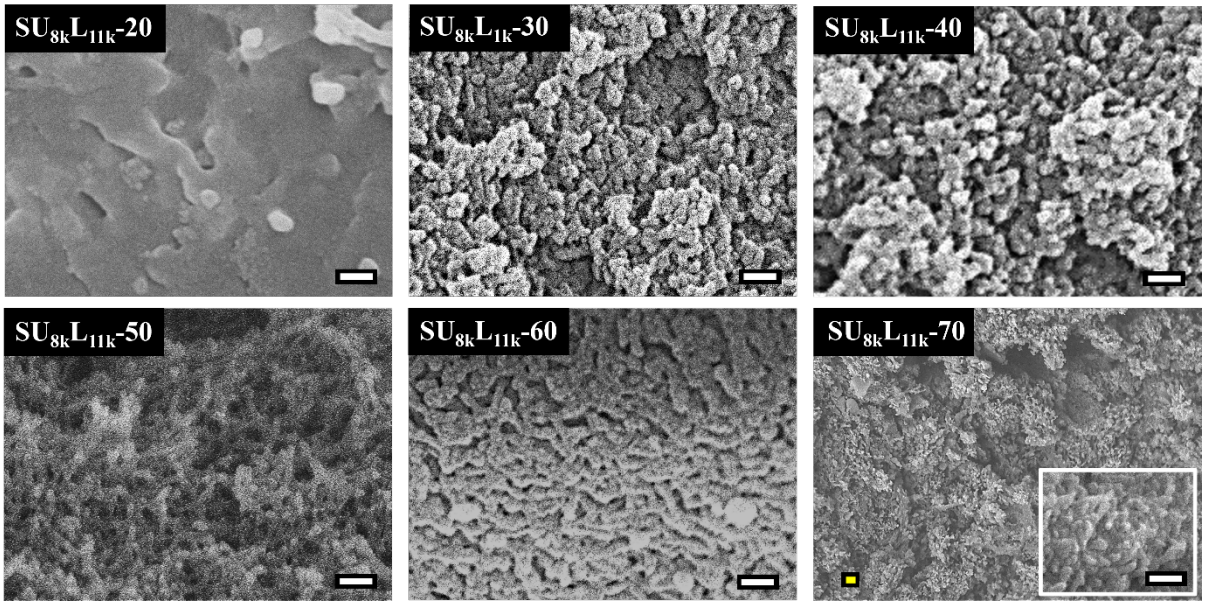

Figure 3. SEM images of $SU_{8k}L_{11k}$ with different compositions after PLA etching. $SU_{8k}L_{11k}$-20 shows almost no porosity due to the PLA phase being enveloped by the PSU matrix, while $SU_{8k}L_{11k}$-30 to $SU_{8k}L_{11k}$-60 exhibit interconnected nanoporous PSU structures with PSU domain sizes of ≈ 30 nm. $SU_{8k}L_{11k}$-70 shows micron-scale voids attributable to the non-percolated nature of PSU, accompanied by nano-domain textures as seen in the inset of a magnified image. White scale bars: 100 nm; yellow: 1 μm.

SEM assisted in understanding the morphology of etched $SU_{8k}L_{11k}$ RECNs (Figure 3). The etched $SU_{8k}L_{11k}$-20 did not show pores since the PSU matrix almost completely encapsulated the minority PLA phase. As a result, the etchant could not access the PLA domains. In contrast, the cocontinuous samples from $SU_{8k}L_{11k}$-30 to $SU_{8k}L_{11k}$-60 after PLA etching showed interconnected nanoporous PSU structures due to percolation of both domains. The

PSU domain size was measured to be ≈ 30 nm, nearly independent of composition. The etched morphology of $SU_{8k}L_{11k}$-70 did not retain the interconnectivity of its nanoporous structures because of the non-percolation of PSU, as evidenced by micron-scale voids in a low magnification SEM image. This observation is consistent with the findings from the decreased scattering intensity in SAXS and the similar Young's modulus to the HT prediction. Nano-domain textures of PSU are observed in a magnified SEM image, although it is difficult to determine whether the nanopores between the PSU domains are preserved. These SEM images further corroborate the identification of the cocontinuous window as described previously.

We aimed to apply interconnected nanoporous PSU samples, similar to those described above, in ultrafiltration applications, owing to their enhanced toughness compared to corresponding interconnected nanoporous PS. Filtration membranes should selectively reject materials that are too large to penetrate the pores, while permitting high permeability of the feed solution through the membrane, however there is inevitably a trade-off between these characteristics, as high permeability requires larger pore sizes, while selectivity demands smaller pore sizes.[5] To minimize the trade-off between permeability and selectivity, it is common to combine a thin membrane with small pore sizes with a thick supporting thick-layer with large pore sizes.[17] Additionally, creating pore connectivity can be beneficial in minimizing dead ends of pores and loss of permeability. For the case of anisotropic cylindrical morphologies, the orientation of pores and a portion of dead-end pores could significantly decrease permeability.[13,54,55] Misoriented (or mixed) orientations increase grain boundaries, inhibiting water transport, and dead-end pores cannot contribute as working pores for filtration. Thus, interconnected nanoporous morphologies have potential to address such issues.

Unfortunately, RECNs, as covalently-crosslinked networks, cannot easily be solution processed to form thin films. To overcome this limitation, we have previously shown that

randomly-linked multiblock polymers (RLMBs), constructed by linking the same constituent strands using difunctional linkers, offer solution-processability, while maintaining a strong propensity to form disordered cocontinuous phases.[40] Thus, we synthesized $SU_{8k}L_{6k}$(M)-50, by using a di-thiol chain extender in thiol-Michael coupling. In this process, the same di-acrylate terminated PSU of 8 kg/mol was combined, this time with a di-acrylate terminated PLA of 6 kg/mol and $Đ = 1.1$ to further ensure targeting a pore size below 50 nm for subsequent filtration testing (Supporting Information, Section 2).

Prior to the fabrication of thin films, we first characterized the bulk-assembly behavior of $SU_{8k}L_{6k}$(M)-50 by gravimetry and SAXS (Figure S10). More than 90 wt. % of PLA was etched, demonstrating robust PLA percolation. No noticeable features were observed by SAXS without PLA etching, just as for the $SU_{8k}L_{11k}$ RECNs. However, a broad shoulder became evident in the scattering pattern around 0.1 nm^{-1} after the etching process. The *d*-spacing was estimated as ≈ 74 nm using TS fitting, though the accuracy of this value might be compromised due to its proximity to the low-*q* limit of the instrument, as only a portion of the characteristic feature could be accurately fit. We spin-coated a solution of $SU_{8k}L_{6k}$(M)-50 onto nanoporous PES substrates, resulting in a ≈ 100 nm film (Figure S11). This thickness was determined by SEM imaging, consistent with methods used in previous studies.[36,56]

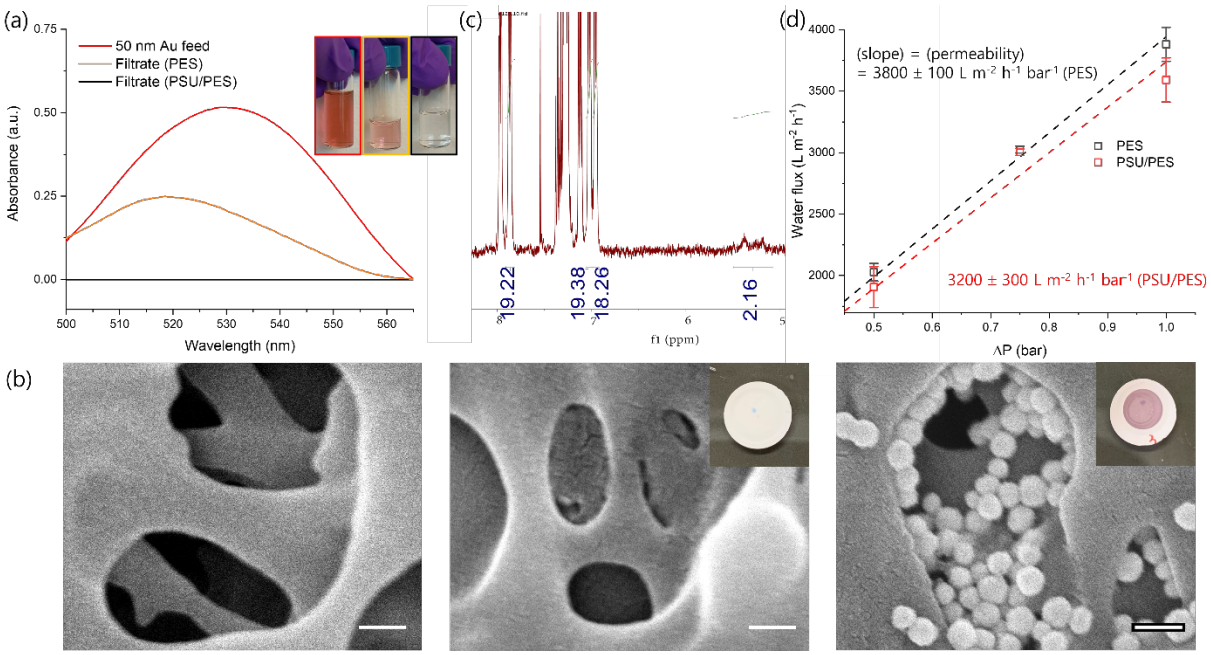

Figure 4. (a) UV-Vis spectra of the feed, containing 0.1 mM of 50 nm Au particles in phosphate buffered saline, and the filtrate. (b) SEM images of the top side of the nascent PES support (left), interconnected nanoporous PSU/supporting PES before (middle), and after Au-nanoparticle filtration (right). The PES pores were filled with PSU, resulting in a thin layer that is impermeable to the Au nanoparticles. (c) NMR spectrum of the $SU_{8k}L_{6k}$(M)-50 after PLA etching, indicating that the PLA was almost fully removed. (d) Permeability of the PES support and PES/PSU membrane. Water flux at each pressure difference was measured in triplicate.

Suspensions of gold (Au) nanoparticles with two different sizes (30 and 50 nm diameters) were selected as feeds, based on the *d*-spacing and expected pore size ($\approx \frac{d}{2} \approx 40$ nm). These suspensions were then passed through the membrane at $\Delta P = 0.5$ bar. The inset image in Figure 4a visually demonstrates the filtration efficiency for 50 nm Au particles. While the feed is pink, the filtrate from the PSU/PES membrane is colorless, indicating successful removal of the particles. Conversely, the light pink color of the filtrate obtained from the

nascent PES membrane suggests a less efficient filtration process. For quantification, we employed UV-Vis spectroscopy to measure the absorbance of the Au nanoparticles in both the feed and filtrate, based on the surface plasmon resonance absorbance in the 500 – 565 nm range (Figure 4a). Rejection rates were determined by comparing the nanoparticle absorbance in the feed with that in the filtrate. These rates were calculated using the formula $100 * (1 - \frac{A_{filtrate}}{A_{feed}})$, where A_{filtrate} and A_{feed} are the absorbance values of the filtrate and the feed, resulting in rejection rates of 52% and ≈ 100%, respectively.

In addition, top-view SEM images of the nascent PES and the PSU/PES membranes before and after Au filtration were captured (Figure 4b). The left image shows the pore size of ≈ 100 nm of the PES supporting substrate on a shiny side (the opposite matte side shows ~ 1 μm pores in Figure S12). Spin-coating of $SU_{8k}L_{6k}$(M)-50 was performed on the shiny side, followed by PLA etching. The selective layer was positioned at the top of the PES support, as shown in the middle. After filtering 50 nm Au particles, they were found to accumulate around the visible PES pores, as they were too large to pass through the PSU pores. This demonstrates that the nascent PES membrane has pore sizes greater than 50 nm, while the PSU selective layer has pore sizes less than 50 nm. However, the filtrate from the PSU/PES membrane, when tested with 30 nm Au particles, maintained a light pink color, indicating only a 52 % rejection (Figure S13). Thus, the PSU/PES membrane demonstrates a size cut-off ranging between 30 - 50 nm.

To quantitatively evaluate the PLA connectivity within the selective layer, we retrieved the interconnected nanoporous PSU thin film from the PES support by selectively dissolving it with chlorobenzene. Following the evaporation of the chlorobenzene, NMR result showed that 93 wt. % of PLA was removed, corresponding to a high degree of PLA percolation (Figure 4c). The permeability of the PSU/PES membrane shows no significant loss in permeability

compared to the PES membrane itself (Figure 4d). It is noteworthy that the interconnected nanoporous PSU layer not only acts as an effective selective layer but also helps in minimizing permeability loss. This largely stems from the control over pore sizes, ≈ 40 nm in this case, coupled with both the small membrane thickness and high degree of pore connectivity, similar to gyroid-based nanoporous membranes described in previous literature.[18]

We used the Hagen-Poiseuille equation to estimate an expected permeability of the nanoporous PSU layer, and indeed found that it is several times larger than that of the PES membrane, consistent with our observation of a negligible decrease in permeability for the bilayer membrane (see Supporting Information, Section 6 for full details). To our knowledge, there has been limited research in developing a thin layer of interconnected nanoporous PSU onto supporting membranes, a process that seeks to achieve a balance of notable selectivity and permeability, while also ensuring mechanical stability. We anticipate that the interconnected nanoporous selective layers formed by microphase separation in RLMBs, which typically yield pores of > 10 nm, will be a complementary addition to the recently reported ultrafiltration membranes with pores of ≈ 10 nm.[36]

4. CONCLUSIONS

We employed two randomly-linked block copolymer architectures, i.e., networks and linear multiblocks, to yield robust formation of disordered cocontinuous nanostructures containing percolated domains of the engineering polymer polysulfone. Subsequent etching of the simultaneously percolated poly(D,L-lactic acid) domains led to mechanically robust interconnected nanoporous polysulfone monoliths and thin films. This system was then employed to construct an ultrafiltration membrane. In this setup, a thin film of the interconnected nanoporous polysulfone was supported by a polyethersulfone membrane, designed to enable size-selective permeation while minimizing permeability loss. In this way, we address the issue of mechanical fragility inherent in earlier work on randomly-linked copolymer architectures composed of brittle polystyrene strands. Additionally, this approach has the potential to overcome challenges in the existing methods of fabricating polysulfone membranes, like non-solvent induced phase separation. These current methods are known for their sensitivity to processing conditions and frequently result in a wide distribution of pore sizes, with limited options for adjusting the pore size precisely. The polysulfone-based cocontinuous nanomaterials and interconnected nanoporous monoliths are anticipated to be suitable for various applications, owing to their adaptability to chemical modification and their superior thermal/mechanical/chemical stabilities.

ASSOCIATED CONTENT

Supporting Information

The Supporting Information is available free of charge at https://pubs.acs.org/doi/xxxxxx. Instruments, materials, experimental methods, Figures S1−S13.

AUTHOR INFORMATION

Corresponding Author

Ryan C. Hayward − Department of Chemical and Biological Engineering, University of Colorado Boulder, Boulder, Colorado 80309, United States; orcid.org/0000-0001-6483-2234; Email: Ryan.Hayward@colorado.edu

Authors

Jaechul Ju – Department of Chemical and Biological Engineering, University of Colorado Boulder, Boulder, Colorado 80309, United States; Email: jaechul.ju@colorado.edu

Funding

This work was supported by the US Department of Energy, through Grant DE-SC0020982.

Notes

The authors declare no competing financial interest.

ACKNOWLEDGMENTS

The authors thank Dr. Na Kyung Kim from the Osuji group at UPenn for her advice in customizing the membrane tester set-up. This work was supported by the U.S. Department of Energy through grant DE-SC0020982.

(1) He, C.; Liu, Z.; Wu, J.; Pan, X.; Fang, Z.; Li, J.; Bryan, B. A. Future Global Urban Water Scarcity and Potential Solutions. *Nat. Commun.* **2021**, *12* (1), 4667. https://doi.org/10.1038/s41467-021-25026-3.
(2) Mekonnen, M. M.; Hoekstra, A. Y. Four Billion People Facing Severe Water Scarcity. *Sci. Adv.* **2016**, *2* (2), e1500323. https://doi.org/10.1126/sciadv.1500323.
(3) Werber, J. R.; Osuji, C. O.; Elimelech, M. Materials for Next-Generation Desalination and Water Purification Membranes. *Nat. Rev. Mater.* **2016**, *1* (5), 16018. https://doi.org/10.1038/natrevmats.2016.18.
(4) Sadeghi, I.; Kaner, P.; Asatekin, A. Controlling and Expanding the Selectivity of Filtration Membranes. *Chem. Mater.* **2018**, *30* (21), 7328–7354. https://doi.org/10.1021/acs.chemmater.8b03334.
(5) Hampu, N.; Werber, J. R.; Chan, W. Y.; Feinberg, E. C.; Hillmyer, M. A. Next-Generation Ultrafiltration Membranes Enabled by Block Polymers. *ACS Nano* **2020**, *14* (12), 16446–16471. https://doi.org/10.1021/acsnano.0c07883.
(6) Yang, S. Y.; Ryu, I.; Kim, H. Y.; Kim, J. K.; Jang, S. K.; Russell, T. P. Nanoporous Membranes with Ultrahigh Selectivity and Flux for the Filtration of Viruses. *Adv. Mater.* **2006**, *18* (6), 709–712. https://doi.org/10.1002/adma.200501500.
(7) Jackson, E. A.; Hillmyer, M. A. Nanoporous Membranes Derived from Block Copolymers: From Drug Delivery to Water Filtration. *ACS Nano* **2010**, *4* (7), 3548–3553. https://doi.org/10.1021/nn1014006.
(8) Guillen, G. R.; Pan, Y.; Li, M.; Hoek, E. M. V. Preparation and Characterization of Membranes Formed by Nonsolvent Induced Phase Separation: A Review. *Ind. Eng. Chem. Res.* **2011**, *50* (7), 3798–3817. https://doi.org/10.1021/ie101928r.
(9) Wang, H. H.; Jung, J. T.; Kim, J. F.; Kim, S.; Drioli, E.; Lee, Y. M. A Novel Green Solvent Alternative for Polymeric Membrane Preparation via Nonsolvent-induced Phase Separation (NIPS). *J. Membr. Sci.* **2019**, *574*, 44-54. https://doi.org/10.1016/j.memsci.2018.12.051.
(10) Zhang, Z.; Rahman, Md. M.; Abetz, C.; Bajer, B.; Wang, J.; Abetz, V. Quaternization of a Polystyrene-Block-Poly(4-Vinylpyridine) Isoporous Membrane: An Approach to Tune the Pore Size and the Charge Density. *Macromol. Rapid Commun.* **2019**, *40* (3), 1800729. https://doi.org/10.1002/marc.201800729.
(11) Abetz, V. Isoporous Block Copolymer Membranes. *Macromol. Rapid Commun.* **2015**, *36* (1), 10–22. https://doi.org/10.1002/marc.201400556.
(12) Jackson, E. A.; Lee, Y.; Hillmyer, M. A. ABAC Tetrablock Terpolymers for Tough Nanoporous Filtration Membranes. *Macromolecules* **2013**, *46* (4), 1484–1491. https://doi.org/ 10.1021/ma302414w.
(13) Phillip, W. A.; Hillmyer, M. A.; Cussler, E. L. Cylinder Orientation Mechanism in Block Copolymer Thin Films Upon Solvent Evaporation. *Macromolecules* **2010**, *43* (18), 7763–7770. https://doi.org/10.1021/ma1012946.
(14) Paradiso, S. P.; Delaney, K. T.; García-Cervera, C. J.; Ceniceros, H. D.; Fredrickson, G. H. Block Copolymer Self Assembly during Rapid Solvent Evaporation: Insights into Cylinder Growth and Stability. *ACS Macro Lett.* **2014**, *3* (1), 16–20. https://doi.org/10.1021/mz400572r.
(15) Hampu, N.; Hillmyer, M. A. Temporally Controlled Curing of Block Polymers in the Disordered State Using Thermally Stable Photoacid Generators for the Preparation of Nanoporous Membranes. *ACS Appl. Polym. Mater.* **2019**, *1* (5), 1148–1154. https://doi.org/10.1021/acsapm.9b00150.
(16) Hampu, N.; Bates, M. W.; Vidil, T.; Hillmyer, M. A. Bicontinuous Porous Nanomaterials from Block Polymers Radically Cured in the Disordered State for Size-Selective

Membrane Applications. *ACS Appl. Nano Mater.* **2019**, *2* (7), 4567–4577.
(17) Vidil, T.; Hampu, N.; Hillmyer, M. A. Nanoporous Thermosets with Percolating Pores from Block Polymers Chemically Fixed above the Order–Disorder Transition. *ACS Cent. Sci.* **2017**, *3* (10), 1114–1120. https://doi.org/10.1021/acscentsci.7b00358.
(18) Park, S.; Kim, Y.; Ahn, H.; Kim, J. H.; Yoo, P. J.; Ryu, D. Y. Giant Gyroid and Templates from High-Molecular-Weight Block Copolymer Self-Assembly. *Sci. Rep.* **2016**, *6* (1), 36326. https://doi.org/10.1038/srep36326.
(19) Shen, K.-H.; Brown, J. R.; Hall, L. M. Diffusion in Lamellae, Cylinders, and Double Gyroid Block Copolymer Nanostructures. *ACS Macro Lett.* **2018**, *7* (9), 1092–1098. https://doi.org/10.1021/acsmacrolett.8b00506.
(20) Peckham, T. J.; Schmeisser, J.; Rodgers, M.; Holdcroft, S. Main-Chain, Statistically Sulfonated Proton Exchange Membranes: The Relationships of Acid Concentration and Proton Mobility to Water Content and Their Effect upon Proton Conductivity. *J. Mater. Chem.* **2007**, *17* (30), 3255. https://doi.org/10.1039/b702339a.
(21) Cochran, E. W.; Garcia-Cervera, C. J.; Fredrickson, G. H. Stability of the Gyroid Phase in Diblock Copolymers at Strong Segregation. *Macromolecules* **2006**, *39* (7), 2449–2451. https://doi.org/10.1021/ma0527707.
(22) Matsen, M. W. Effect of Architecture on the Phase Behavior of AB-Type Block Copolymer Melts. *Macromolecules* **2012**, *45* (4), 2161–2165. https://doi.org/10.1021/ma202782s.
(23) Bates, F. S.; Maurer, W. W.; Lipic, P. M.; Hillmyer, M. A.; Almdal, K.; Mortensen, K.; Fredrickson, G. H.; Lodge, T. P. Polymeric Bicontinuous Microemulsions. *Phys. Rev. Lett.* **1997**, *79* (5), 849–852. https://doi.org/10.1103/PhysRevLett.79.849.
(24) Hoehn, B. D.; Kellstedt, E. A.; Hillmyer, M. A. Tough Polycyclooctene Nanoporous Membranes from Etchable Block Copolymers. *Soft Matter* **2024**, *20* (2), 437–448. https://doi.org/10.1039/D3SM01498C.
(25) Widin, J. M.; Schmitt, A. K.; Schmitt, A. L.; Im, K.; Mahanthappa, M. K. Unexpected Consequences of Block Polydispersity on the Self-Assembly of ABA Triblock Copolymers. *J. Am. Chem. Soc.* **2012**, *134* (8), 3834–3844. https://doi.org/10.1021/ja210548e.
(26) Yan, Y.; Huang, J.; Tang, B. Z. Kinetic Trapping – a Strategy for Directing the Self-Assembly of Unique Functional Nanostructures. *Chem. Commun.* **2016**, *52* (80), 11870–11884. https://doi.org/10.1039/C6CC03620A.
(27) Yang, J.; Wang, X.-L.; Tian, Y.; Lin, Y.; Tian, F. Morphologies and Crystalline Forms of Polyvinylidene Fluoride Membranes Prepared in Different Diluents by Thermally Induced Phase Separation. *J. Polym. Sci. Part B Polym. Phys.* **2010**, *48* (23), 2468–2475. https://doi.org/10.1002/polb.22145.
(28) Lee, J. T.; Jo, C.; De Volder, M. Bicontinuous Phase Separation of Lithium-Ion Battery Electrodes for Ultrahigh Areal Loading. *Proc. Natl. Acad. Sci.* **2020**, *117* (35), 21155–21161. https://doi.org/10.1073/pnas.2007250117.
(29) Cui, Z.; Hassankiadeh, N. T.; Lee, S. Y.; Lee, J. M.; Woo, K. T.; Sanguineti, A.; Arcella, V.; Lee, Y. M.; Drioli, E. Poly(Vinylidene Fluoride) Membrane Preparation with an Environmental Diluent via Thermally Induced Phase Separation. *J. Membr. Sci.* **2013**, *444*, 223–236. https://doi.org/10.1016/j.memsci.2013.05.031.
(30) Wu, Y.-H.; Lo, T.-Y.; She, M.-S.; Ho, R.-M. Morphological Evolution of Gyroid-Forming Block Copolymer Thin Films with Varying Solvent Evaporation Rate. *ACS Appl. Mater. Interfaces* **2015**, *7* (30), 16536–16547. https://doi.org/10.1021/acsami.5b03977.
(31) Sakurai, S.; Sakamoto, J.; Shibayama, M.; Nomura, S. Effects of Microdomain

Structures on the Molecular Orientation of Poly(Styrene-Block-Butadiene-Block-Styrene) Triblock Copolymer. *Macromolecules* **1993**, *26* (13), 3351–3356. https://doi.org/10.1021/ma00065a018.

(32) Hernandez, J. J.; Zhang, H.; Chen, Y.; Rosenthal, M.; Lingwood, M. D.; Goswami, M.; Zhu, X.; Moeller, M.; Madsen, L. A.; Ivanov, D. A. Bottom-Up Fabrication of Nanostructured Bicontinuous and Hexagonal Ion-Conducting Polymer Membranes. *Macromolecules* **2017**, *50* (14), 5392–5401. https://doi.org/10.1021/acs.macromol.6b02674.

(33) Samitsu, S.; Zhang, R.; Peng, X.; Krishnan, M. R.; Fujii, Y.; Ichinose, I. Flash Freezing Route to Mesoporous Polymer Nanofibre Networks. *Nat. Commun.* **2013**, *4* (1), 2653. https://doi.org/10.1038/ncomms3653.

(34) Seo, M.; Hillmyer, M. A. Reticulated Nanoporous Polymers by Controlled Polymerization-Induced Microphase Separation. *Science* **2012**, *336* (6087), 1422–1425. https://doi.org/10.1126/science.1221383.

(35) Hampu, N.; Hillmyer, M. A. Molecular Engineering of Nanostructures in Disordered Block Polymers. *ACS Macro Lett.* **2020**, *9* (3), 382–388. https://doi.org/10.1021/acsmacrolett.0c00036.

(36) Chan, W. Y.; Hillmyer, M. A. Disordered Triblock Polymers for Nanoporous Materials with Tunable Surface Properties for Ultrafiltration Applications. *ACS Appl. Polym. Mater.* **2022**, acsapm.2c00065. https://doi.org/10.1021/acsapm.2c00065.

(37) Zeng, D.; Ribbe, A.; Hayward, R. C. Anisotropic and Interconnected Nanoporous Materials from Randomly End-Linked Copolymer Networks. *Macromolecules* **2017**, *50* (12), 4668–4676. https://doi.org/10.1021/acs.macromol.7b00007.

(38) Zeng, D.; Ribbe, A.; Kim, H.; Hayward, R. C. Stress-Induced Orientation of Cocontinuous Nanostructures within Randomly End-Linked Copolymer Networks. *ACS Macro Lett.* **2018**, *7* (7), 828–833. https://doi.org/10.1021/acsmacrolett.8b00453.

(39) Zeng, D.; Hayward, R. C. Effects of Randomly End-Linked Copolymer Network Parameters on the Formation of Disordered Cocontinuous Phases. *Macromolecules* **2019**, *52* (7), 2642–2650. https://doi.org/10.1021/acs.macromol.9b00050.

(40) Zeng, D.; Gupta, R.; Coughlin, E. B.; Hayward, R. C. Assembly of Disordered Cocontinuous Morphologies by Multiblock Copolymers with Random Block Sequence and Length Dispersity. *ACS Appl. Polym. Mater.* **2020**, acsapm.0c00428. https://doi.org/10.1021/acsapm.0c00428.

(41) Abdelrasoul, A.; Doan, H.; Lohi, A.; Cheng, C.-H. Morphology Control of Polysulfone Membranes in Filtration Processes: A Critical Review. *ChemBioEng Rev.* **2015**, *2* (1), 22–43. https://doi.org/10.1002/cben.201400030.

(42) Viswanathan, R.; Johnson, B. C.; McGrath, J. E. Synthesis, Kinetic Observations and Characteristics of Polyarylene Ether Sulphones Prepared via a Potassium Carbonate DMAC Process. *Polymer* **1984**, *25* (12), 1827–1836. https://doi.org/10.1016/0032-3861(84)90258-1.

(43) Linares, A.; Acosta, J. L. Structural Characterization of Polymer Blends Based on Polysulfones. *J. Appl. Polym. Sci.* **2004**, *92* (5), 3030–3039. https://doi.org/10.1002/app.20263.

(44) Affdl, J. C. H.; Kardos, J. L. The Halpin-Tsai Equations: A Review. *Polym. Eng. Sci.* **1976**, *16* (5), 344–352. https://doi.org/10.1002/pen.760160512.

(45) Luo, Z.; Li, X.; Shang, J.; Zhu, H.; Fang, D. Modified Rule of Mixtures and Halpin–Tsai Model for Prediction of Tensile Strength of Micron-Sized Reinforced Composites and Young's Modulus of Multiscale Reinforced Composites for Direct Extrusion Fabrication. *Adv. Mech. Eng.* **2018**, *10* (7), 1687814018785286.

https://doi.org/10.1177/1687814018785286.
(46) Nelson, K.; Kelly, C. N.; Gall, K. Effect of Stress State on the Mechanical Behavior of 3D Printed Porous Ti6Al4V Scaffolds Produced by Laser Powder Bed Fusion. *Mater. Sci. Eng. B* **2022**, *286*, 116013. https://doi.org/10.1016/j.mseb.2022.116013.
(47) De Carolis, S.; Putignano, C.; Soria, L.; Carbone, G. Effect of Porosity and Pore Size Distribution on Elastic Modulus of Foams. *Int. J. Mech. Sci.* **2024**, *261*, 108661. https://doi.org/10.1016/j.ijmecsci.2023.108661.
(48) Teubner, M.; Strey, R. Origin of the Scattering Peak in Microemulsions. *J. Chem. Phys.* **1987**, *87* (5), 3195–3200. https://doi.org/10.1063/1.453006.
(49) Zheng, C.; Zhang, B.; Bates, F. S.; Lodge, T. P. Self-Assembly of Partially Charged Diblock Copolymer-Homopolymer Ternary Blends. *Macromolecules* **2022**, *55* (11), 4766–4775. https://doi.org/10.1021/acs.macromol.2c00518.
(50) Chen, S. H.; Chang, S. L.; Strey, R. On the Interpretation of Scattering Peaks from Bicontinuous Microemulsions. In *Trends in Colloid and Interface Science IV*; Zulauf, M., Lindner, P., Terech, P., Eds.; Progress in Colloid & Polymer Science; Steinkopff: Darmstadt, 1990; Vol. 81, pp 30–35. https://doi.org/10.1007/BFb0115519.
(51) Morkved, T. L.; Stepanek, P.; Krishnan, K.; Bates, F. S.; Lodge, T. P. Static and Dynamic Scattering from Ternary Polymer Blends: Bicontinuous Microemulsions, Lifshitz Lines, and Amphiphilicity. *J. Chem. Phys.* **2001**, *114* (16), 7247–7259. https://doi.org/10.1063/1.1357800.
(52) Gompper, G.; Schick, M. Scattering from Internal Interfaces in Microemulsion and Sponge Phases. *Phys. Rev. E* **1994**, *49* (2), 1478–1482. https://doi.org/10.1103/PhysRevE.49.1478.
(53) Strey, R.; Winkler, J.; Magid, L. Small-Angle Neutron Scattering from Diffuse Interfaces. 1. Mono- and Bilayers in the Water-Octane-Pentaoxyethylene Monododecyl Ether (C12Es) System. *J. Phys. Chem.* **1991**, *95* (19), 7502–7507. https://doi.org/10.1021/j100172a070.
(54) Phillip, W. A.; O'Neill, B.; Rodwogin, M.; Hillmyer, M. A.; Cussler, E. L. Self-Assembled Block Copolymer Thin Films as Water Filtration Membranes. *ACS Appl. Mater. Interfaces* **2010**, *2* (3), 847–853. https://doi.org/10.1021/am900882t.
(55) Querelle, S. E.; Jackson, E. A.; Cussler, E. L.; Hillmyer, M. A. Ultrafiltration Membranes with a Thin Poly(Styrene)-b-Poly(Isoprene) Selective Layer. *ACS Appl. Mater. Interfaces* **2013**, *5* (11), 5044–5050. https://doi.org/10.1021/am400847m.
(56) Hampu, N.; Werber, J. R.; Hillmyer, M. A. Co-Casting Highly Selective Dual-Layer Membranes with Disordered Block Polymer Selective Layers. *ACS Appl. Mater. Interfaces* **2020**, *12* (40), 45351–45362. https://doi.org/10.1021/acsami.0c13726.

TOC

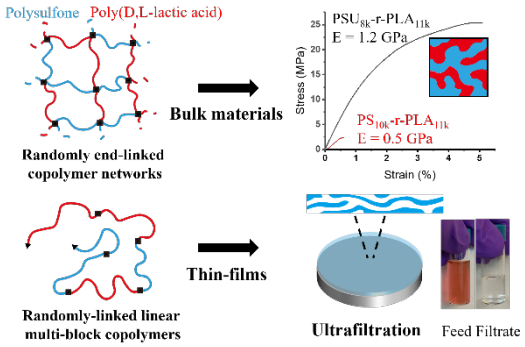
Polysulfone
Poly(D,L-lactic acid)
Bulk materials
Randomly end-linked copolymer networks
PSU8k-r-PLA11k
E = 1.2 GPa
PS10k-r-PLA11k
E = 0.5 GPa
Stress (MPa)
Strain (%)
Thin-films
Randomly-linked linear multi-block copolymers
Ultrafiltration
Feed Filtrate